PROCEEDINGS OF SCIENCE

Exploring possible γ-Ray Emission in polar magnetic CVs using Fermi LAT data

Spencer. T. Madzime[a,*] **and P.J. Meintjes**[a]

[a] *University of the Free State,*
205 Nelson Mandela Dr, Park West, Bloemfontein, South Africa

E-mail: tsmadzime@gmail.com, MeintjPJ@ufs.ac.za

Polar (AM Herculis) systems, a subclass of Magnetic Cataclysmic Variables (MCVs), exhibit unique characteristics such as strong magnetic fields ranging from 10 to 230 MG, phase-locked rotation, and orbital periods devoid of accretion disks. These systems are known for emitting strong X-rays, UV radiation, infrared radiation, and polarized light. The potential candidacy of polar systems for gamma-ray emissions have been explored. In this study, we present preliminary analysis of Fermi LAT data in the energy range of 0.1-500 GeV, focusing on the detection of gamma-ray emissions and pulsed signals associated with the orbital periods of specific sources. Using a binned likelihood analysis technique, we initially observed soft count spectra, hinting a potential emissions at a lower energy levels. Further narrowing our focus to the energy range of 50 MeV-20 GeV, we identified sources with test statistics (TS) exceeding the Fermi detection threshold. Subsequently, we explored the possibility of pulsed emissions modulated to the orbital period of these systems. We present pulsed emission results for sources WW Hor (P_{orb} = 115.5 mins; - log Prob = 5,397, EXO 023432-5237.3), EF Eridani (P_{orb} = 81 mins; - log Prob = 5.842), EU UMa (P_{orb} = 90 mins; - log Prob = 4.133), AR UMa (P_{orb} = 115.6 mins; - log Prob = 4.557), and V834 Cen (P_{orb} = 101.5 mins; - log Prob = 4.450, E1405-451). The search for periodic emission revealed evidence of pulsed emission at the orbital period within a 0.6° region of interest. We detected gamma-ray pulsations with significance above 4 σ in all sources. Since we used ephemerides derived from optical or X-rays, continuous monitoring of these sources to improve their ephemerides may improve our results.

High Energy Astrophysics in Southern Africa 2023 (HEASA 2023)
September 5 - 9, 2023
Mtunzini, KwaZulu-Natal, South Africa

*Speaker

PoS(HEASA2023)021

1. Introduction

Magnetic Cataclysmic Variables (magnetic CVs) constitute a unique class of binary systems where a strong magnetic field significantly influences the transfer of mass and the process of mass accretion, leading to emissions across all wavelengths. These systems are classified into two main subgroups based on the strength of their magnetic fields: polars and intermediate polars (IPs). Polars are highly magnetized magnetic CVs, with the primary star's magnetic field strength exceeding 10 Mega Gauss (MG) e.g., [1] . On the other hand, intermediate polars (IPs) have magnetic field strengths ranging from 1 to 10 MG ([2, 3]). The interests of this paper focuses on possible gamma-ray emission in polars and associated particle acceleration mechanism.

Polars, also known as AM Herculis (AM Her) systems, are unique binary systems characterized by the absence of an accretion disk due to the disruptive influence of the primary star's strong magnetic field. The magnetosphere of the white darf extends beyond the circularisation radius, connecting with the secondary star's magnetic field. Synchronized spin and orbital periods are distinctive features ([4, page 361, 470-471], [5]). The primary star's dominant magnetic field forces synchronization with its spin, directing mass transfer along magnetic field lines ([4]). The supersonic mass stream, upon passing a shock above the primary star's surface, releases gravitational potential energy, generating hard X-rays ([6]). This, along with soft X-rays produced by the heated surface, distinguishes polars systems, exhibiting cyclotron radiation, strong polarization, and infrared emission e.g., [7].

The inspiration for this study came from the recent detection of potential transient low-level gamma-ray emissions in magnetic cataclysmic binary systems [8–11]. The list of sources was adopted form a list of polars that were selected for follow-up study with NICER [12] (P.I. Kaya Mori, Columbia Astrophysics Laboratory, Columbia University, New York, NY 10027, USA (personal communication)). The structure of this contribution paper is outlined as follows: a concise review of particle acceleration in polar systems is presented in the subsequent section. The following parts cover the acquisition and analysis of Fermi-LAT data, the presentation of preliminary results for each source, and, finally, a section dedicated to discussion and conclusions.

2. Particle Acceleration Mechanism in Polar systems

It has been suggested that deviations from synchronous rotation play a crucial role in the generation of substantial potentials, consequently, particle acceleration in these systems [1] to explain radio emissions from AM Her systems. It should be noted that the deviation from synchronous considered here is very small and not detectable. This mechanism is known as unipolar inductor, where a small asynchronous rotation leads to huge potential differences being established across flux tubes which link the primary and secondary star. We will demonstrate that deviations from synchronous rotation, commonly referred to as nutations, may result in the companion star functioning as a unipolar inductor. Such a scenario has the potential to generate significant potential differences across the companion star, thereby establishing the required mechanism for particle acceleration to higher energies, which may explain possible gamma-rays in polar systems.

Assuming a dipolar configuration for white dwarf magnetic field $B_{WD} = 5 \times 10^7$ G, the magnetic field experienced by the companion star is given by $B(r) = 5 \times 10^7 R_{wd,9} d_9^{-3}$ G [1]. Here,

the radius of the white dwarf is considered to be 10^9 cm, and the separation between the two stars is defined by d_9. Chanmugam and Dulk [1] derived the potential difference resulting from the induced electric field perceived by the companion. This induced electric field expressed as $E = -\frac{V \times B}{c}$ e.g., [13], with $V = V_{\rm orb} - V_{\rm corot}$. This can be expressed in terms of a asynchronicity parameter $V \sim d\zeta$. In this context, $V_{\rm orb}$ represents the orbital velocity of the companion star, while $V_{\rm corot}$ represents the velocity of the magnetic flux tubes co-rotating with the white dwarf. The slightest mismatch between the motion of the flux tubes of the white dwarf anchored in the secondary star will induce a departure from synchronicity ζ, which is instrumental in inducing huge field aligned potentials. Therefore,

$$E = 5 \times 10^8 \, \zeta \, d_9^{-2} \left[\frac{B_{wd}}{50\,\mathrm{MG}} \right] \text{ Volts cm}^{-1}.$$

In the case where the companion has a diameter $D \sim 10^{10}$ cm with D_{10}, the resulting potential difference across it can be expressed as

$$\Phi = 5 \times 10^{18} \, \zeta \, d_9^{-2} \, D_{10} \text{ Volts}.$$

Therefore, by setting $d_9 = d/10^9 \approx 70$ to achieve potential differences of $\Phi \sim 100$ GV for $\zeta \sim 10^{-4}$ rad s^{-1}. If the system possesses this slight asynchronism and fulfils the other conditions discussed by Chanmugam and Dulk [1], the potential energy required to accelerate particles to account for gamma-rays with energies up to 20 GeV. This possibility could provide an explanation for the soft gamma rays observed in polar systems. Gamma ray emission may occur through leptonic (Inverse-Compton) and hadronic ($\pi^\circ - decay$) processes.

3. Observation & Analysis of Fermi-LAT data.

The Fermi Gamma-Ray Space Telescope was launched on June 11, 2008 into its low-Earth orbit, and has been consistently delivering high-quality gamma-ray data. Fermi's primary instrument, is the Large Area Telescope (LAT). The LAT functions as a pair conversion telescope, boasting an expansive field of view of approximately 2.4 sr, making it sensitive to gamma rays ranging from around 20 MeV up to over 1 TeV [14, 15]. For this study, a dataset spanning 14 years (start of Fermi LAT mission and 2022-03-25 at 05:21:17) of publicly available Pass 8 [15] LAT data is utilized.

The selection process involves choosing photons with energies ranging from 100 MeV to 500 GeV, 50 MeV to 20 GeV, and 500 MeV to 20 GeV within a defined Region of Interest (ROI) centered on the specific source under investigation. The response (P8R3_SOURCE_V2_v1) function, and corresponding source-class events (evclass=128) and FRONT+BACK event type (evtype=3) were used to filter plausible events within 10 degrees ROI. To enhance data quality, we restrict our data selection to zenith angles less than 90°, effectively eliminating photons originating from the Earth limb (Limb Brightening). Utilizing gtmktime, we obtain time intervals during which the LAT operated in its nominal science operations mode, excluding periods coinciding with gamma-ray bursts and solar flares. The data is then binned into 20 logarithmically spaced bins in energy, employing a spatial binning of 0.1° per pixel. Our analytical approach incorporates all sources documented in the most recent Fermi catalogue of point-like and extended sources [16]. Additionally, we integrate

the standard diffuse Galactic foreground emission model recommended for point source analysis. To account for extragalactic diffuse gamma-ray background and misclassified cosmic rays, a spatially isotropic model is included. The normalizations of both the Galactic and extragalactic diffuse emission models are treated as free parameters in the binned maximum likelihood [17] analysis performed using gtlike, pyLikelihood, and fermipy of the Fermi Science Tools software packages (v11r0p5).

The Fermi LAT considers events from the front within the energy range of 0.1-100 GeV for its initial detection, a strategy aimed at mitigating the risk of false detections given that events below 100 MeV could primarily consist of background photons. While effective, this approach presents a challenge for sources emitting soft gamma rays below 50 GeV. To address this, we conducted a thorough examination of potential pulsed gamma-ray signals in Fermi-LAT gamma-ray data, corroborating our results obtained through binned likelihood analysis. Our investigative approach involved employing the Rayleigh test and the Fermi plug-in [18], utilizing the TEMPO2 [19] radio timing analysis tool. Specifically, Fermi-LAT photon events within the energy range of 50 MeV-20 GeV were considered, extracted from a Region of Interest (ROI) with a radius of 0.6 degrees around each source. We applied the Fermi-LAT event selection process (*gtselect* and *gmktime*) to curate all events related to the source of interest. The *gtpsearch* routine in Fermi tools (version 10) was then employed for photon event folding using the Rayleigh folding analysis algorithm and the ephemeris. Furthermore, data was phased using the peak period from *gtpsearch* and the appropriate ephemeris through the Fermi plug-in, enhancing the precision of our analysis. Events were barycentred on the fly using the *gtpsearch* tool of the Fermi science tools (version v10). Tempo2 and the Fermi plug-in integrate built-in capabilities for conducting barycentric correction, provided essential parameters such as the source position and the spacecraft file are supplied.

4. Results

The examination of Fermi Large Area Telescope (LAT) data in the energy range of 0.1-500 GeV has unveiled interesting results of possible gamma-ray emissions from polar systems. Soft count spectra were initially observed, hinting a potential low level emissions at a lower energy e.g., below 20 GeV. A more focused analysis in the range of 50 MeV-20 GeV revealed several sources exceeding the Fermi detection threshold (TS>25). Table 1 summarizes the test statistics (TS), predicted counts (Npred), and integral flux (photons $cm^{-2}s^{-1}$) for the listed polar systems. In-depth binned likelihood analysis and exploration of pulsed emission modulated to the orbital period further exposed evidence of significant gamma-ray emissions. Noteworthy sources, including WW Hor , EF Eridani, EU UMa, AR UMa, and V834 Cen, exhibited compelling features in their Rayleigh test power spectra, H-test plots, and gamma-ray phase light curves. The Rayleigh test power spectra and H-test plots also reveal that the pulsed signal significance is above 4 σ. The details of each source's characteristics, including their respective ephemerides and timing analyses will be presented.

4.1 WW Hor

WW Hor was initially observed as an unexpected X-ray source during an EXOSAT survey and later recognized as a polar system, with an orbital period in the interval of 113-115 minutes [20]. Bailey et al. [21] managed to refine the orbital period (115.5 minutes). We searched for possible

Name	Ts	Npred	Integral Flux [photons $cm^{-2}s^{-1}$]	Flux Error [photons $cm^{-2}s^{-1}$]
EF Eri	41.75	2186.66	4.89e-09	7.78e-10
WW Hor	78.83	3634.63	6.92e-09	8.08e-10
V834 Cen	36.98	3859.98	7.80e-09	1.43e-09
EU UMa	27.86	2222.35	4.90e-09	1.03e-09
AR UMa	30.22	2036.83	3.91e-09	8.09e-10
CE Gru	26.71	1462.27	3.59e-09	7.76e-10
BL Hyi	32.72	1502.55	3.32e-09	6.40e-10
CV Hyi	53.24	2939.36	5.86e-09	9.08e-10
UW Pic	86.82	4515.11	8.57e-09	9.80e-10
RS Cae	25.95	2255.79	4.28e-09	8.48e-10
MT Dra	47.16	3088.21	5.19e-09	5.30e-10
MQ Dra	29.90	2314.47	3.76e-09	7.40e-10
EV UMa	35.92	1581.15	2.95e-09	5.57e-10

Table 1: The results (Energy range 50 MeV - 20 GeV) of this study are preliminary and the results of the search for orbital modulation of the sources in red will be presented. For the other sources in black only an initial binned analysis was conducted. First column is the name of the source, followed by test statistics (TS), which is associated with significance level of the source. The number of predicted counts (Npred) is presented in the third column. The integral flux and error are in the units photons $cm^{-2}s^{-1}$. The list of sources was adopted form a list of polars that were selected for follow-up study with NICER [12] (P.I. Kaya Mori, Columbia Astrophysics Laboratory, Columbia University, New York, NY 10027, USA (personal communication))

steady gamma-ray emission and periodic oscillations in the energy range 50 MeV-20 GeV. The observed counts map, model counts map, and residual map of the source WW Hor are illustrated in Figure 1. In the model map, all significant sources are included, showing their predicted counts. The residual map indicates the goodness of fit, with extreme negative or positive counts indicating discrepancies between predicted and observed counts. The Rayleigh test power spectrum of WW Hor , H-test plot with TS accumulated from the start of the mission plotted as a function of time, and gamma-ray phase light curve of WW Hor in the energy range 50 MeV-20 GeV, with photons extracted from a ROI with a radius of 0.6 degrees folded at the orbital period with [21] ephemeris (T_0 = 2447126.207969 BJD) are displayed in Figure 2. The Rayleigh test power spectrum reveals a peak corresponding to the orbital period of WW Hor. The probability associated with this observation, indicating the likelihood of it occurring by chance, is approximately $P \sim 4.0047\times10^{-6}$. Consequently, the null hypothesis, suggesting the absence of pulsed emission at the orbital period, is rejected with a level of confidence at 99.99959953%.

4.2 EF Eridani

The orbital period of EF Eridani is 81 minutes e.g., [22, 23]. We searched for possible steady gamma-ray and periodic oscillations from EF Eridani in the energy range 50 MeV-20 GeV. The observed counts map, model counts map, and residual map of the source EF Eridani are illustrated

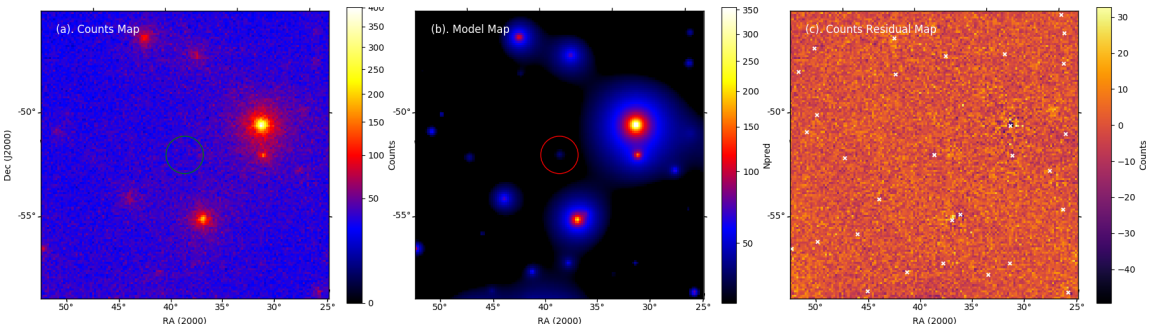

Figure 1: Displayed from the left is observed counts map of the source WW Hor , the middle is the model counts map, and on the last panel is the residual map. All significant sources included in the model will show with their predicted counts in the model map. The residual map display the goodness of the fit. The difference between predicted and observed counts is reflected as either negative or positive counts at the locations where counts are underestimated or overestimated.

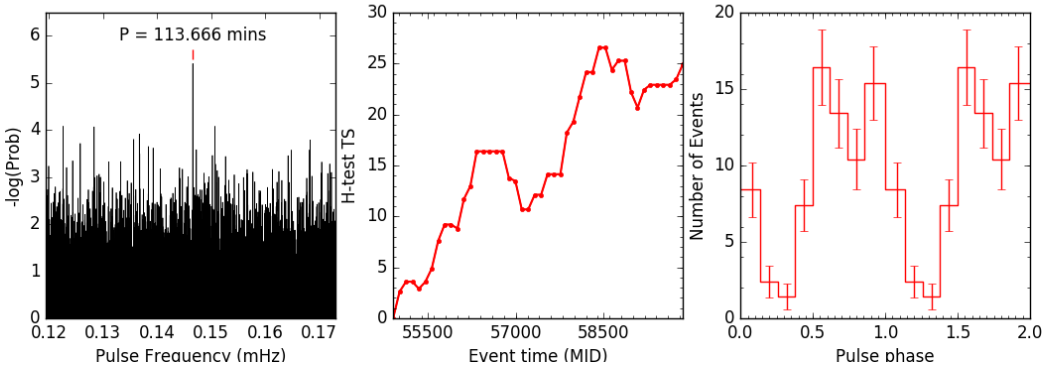

Figure 2: WW Hor - Left: Rayleigh test power spectrum. Middle: H-test plot showing TS accumulation over time. Right: Gamma-ray phase light curve of WW Hor (0.5-10 GeV), folded with Beuermann et al. (1986) ephemeris using photons from a 0.6° radius ROI.

in Figure 3. Figure 4 display Rayleigh test power spectrum, H-test plot, and gamma-ray phase light curve of EF Eridani, folded at the orbital period of EF Eridani with the ephemeris (T_0 = 2443945.00806595 BJD, [24]). The Rayleigh test power spectrum reveals a peak corresponding to the orbital period of EF Eridani. The probability associated with this observation, indicating the likelihood of it occurring by chance, is approximately $P \sim 1.4395 \times 10^{-6}$. Consequently, the null hypothesis, suggesting the absence of pulsed emission at the orbital period, is rejected with a level of confidence at 99.99985605%.

4.3 EU UMa

The orbital period was estimated to be 90±0.2 min according to optical spectroscopic and photometric observations [25]. We searched for possible steady gamma-ray and periodic oscillations from EU UMa in the energy range 50 MeV-20 GeV. The observed counts map, model counts map, and residual map of the source EU UMa are illustrated in Figure 5. Figure 6 display Rayleigh test power spectrum, H-test plot, and gamma-ray phase light curve of EU UMa, folded at the

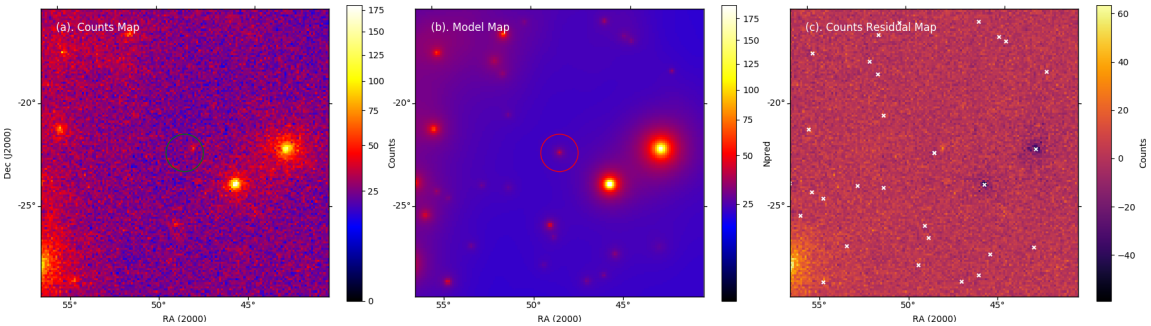

Figure 3: Displayed from the left is observed counts map of the source EF Eridani, the middle is the model counts map, and on the last panel is the residual map. All significant sources included in the model will show with their predicted counts in the model map. The residual map display the goodness of the fit. The difference between predicted and observed counts is reflected as either negative or positive counts at the locations where counts are underestimated or overestimated.

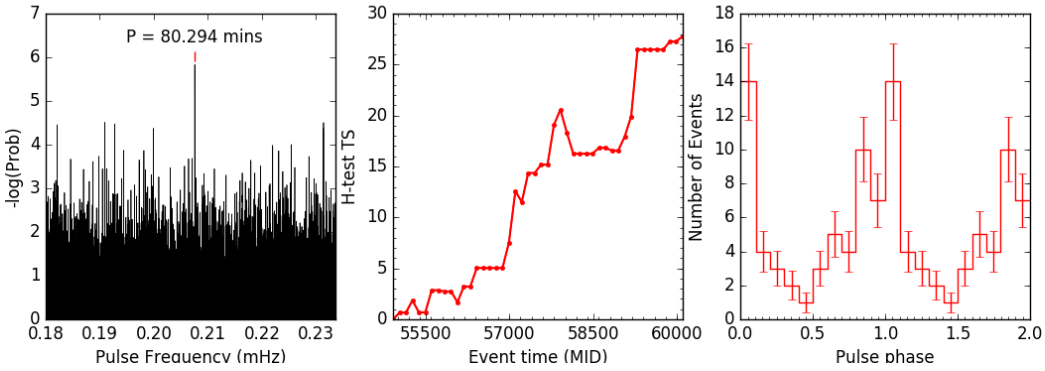

Figure 4: EF Eridani - Left: Rayleigh test power spectrum. Middle: H-test plot showing TS accumulation over time. Right: Gamma-ray phase light curve folded with Schwope and Christensen (2010) ephemeris.

90 mins orbital period of EU UMa with the ephemeris (T_0 = 2449042.66985 BJD, [26]). The Rayleigh test power spectrum reveals a peak corresponding to the orbital period of EU UMa. The probability associated with this observation, indicating the likelihood of it occurring by chance, is approximately $P \sim 2.7676 \times 10^{-5}$. Consequently, the null hypothesis, suggesting the absence of pulsed emission at the orbital period, is rejected with a level of confidence at 99.9972324%.

4.4 AR UMa

The orbital period of AR UMa is 115.6 mins, e.g., [2]. We searched for possible steady gamma-ray and periodic oscillations from AR UMa in the energy range 50 MeV-20 GeV. The observed counts map, model counts map, and residual map of the source AR UMa are illustrated in Figure 7. Figure 8 display Rayleigh test power spectrum, H-test plot, and gamma-ray phase light curve of AR UMa, folded at the orbital period of AR UMa with the ephemeris (T_0 = 2450470.51140074 BJD, [2]). The Rayleigh test power spectrum reveals a peak corresponding to the orbital period of AR UMa. The probability associated with this observation, indicating the likelihood of it occurring by chance, is approximately $P \sim 7.3475 \times 10^{-5}$. Consequently, the null hypothesis, suggesting

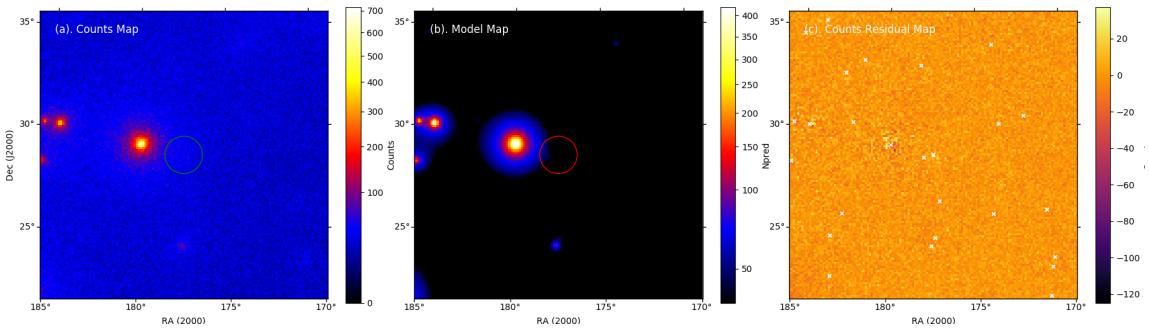

Figure 5: Displayed from the left is observed counts map of the source EU UMa, the middle is the model counts map, and on the last panel is the residual map. All significant sources included in the model will show with their predicted counts in the model map. The residual map display the goodness of the fit. The difference between predicted and observed counts is reflected as either negative or positive counts at the locations where counts are underestimated or overestimated.

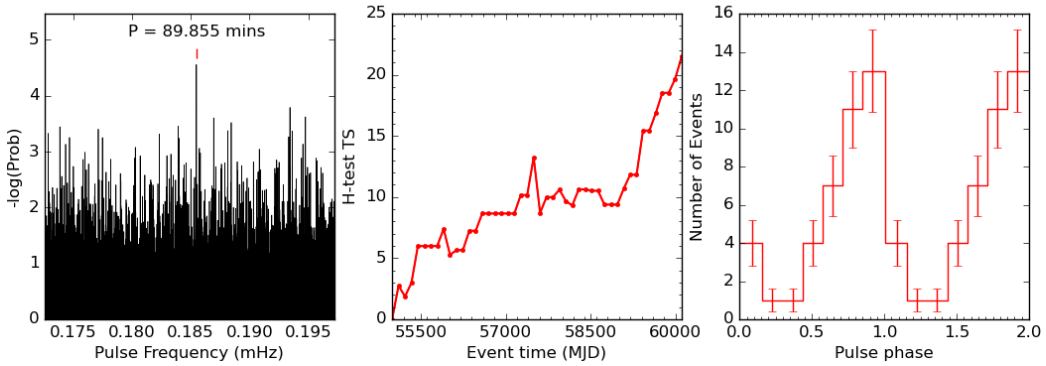

Figure 6: EU UMa - Left: Rayleigh test power spectrum. Middle: H-test plot showing TS accumulation over time. Right: Gamma-ray phase light curve folded with Howell et al. [26] 90 mins timing ephemeris using photons from a 0.6° radius ROI.

the absence of pulsed emission at the orbital period, is rejected with a level of confidence at 99.9926525%.

4.5 V834 Cen

The orbital period of V834 Cen is 101.5 mins [27]). We searched for possible steady gamma-ray and periodic oscillations from V834 Cen in the energy range 50 MeV-20 GeV. The observed counts map, model counts map, and residual map of the source V834 Cen are illustrated in Figure 9. Figure 10 display Rayleigh test power spectrum, H-test plot, and gamma-ray phase light curve of V834 Cen, folded at the orbital period of V834 Cen with the ephemeris (T_0 = 2445048.07049723 BJD, [27]). The Rayleigh test power spectrum reveals a peak corresponding to the orbital period of V834 Cen. The probability associated with this observation, indicating the likelihood of it occurring by chance, is approximately $P \sim 3.5446 \times 10^{-5}$. Consequently, the null hypothesis, suggesting the absence of pulsed emission at the orbital period, is rejected with a level of confidence at 99.9964554%.

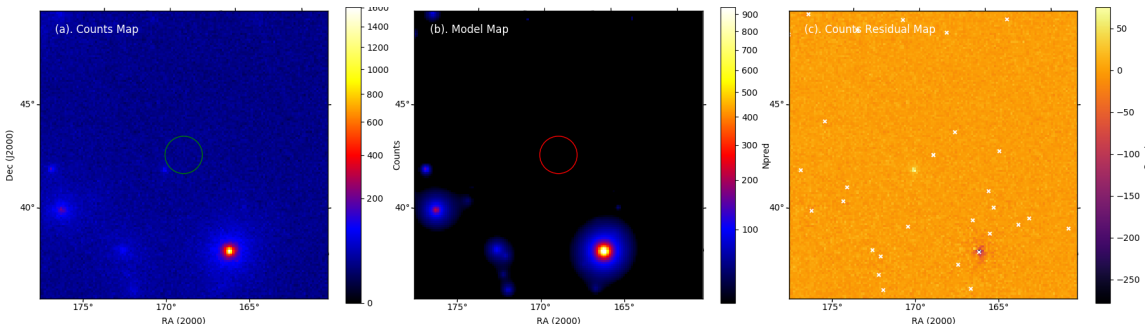

Figure 7: Displayed from the left is observed counts map of the source AR UMa, the middle is the model counts map, and on the last panel is the residual map. All significant sources included in the model will show with their predicted counts in the model map. The residual map display the goodness of the fit. The difference between predicted and observed counts is reflected as either negative or positive counts at the locations where counts are underestimated or overestimated.

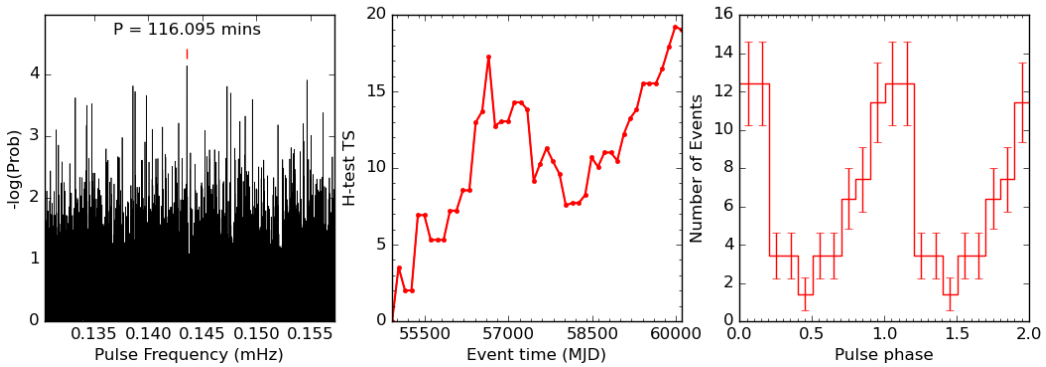

Figure 8: AR UMa - Left: Rayleigh test power spectrum. Middle: H-test plot showing TS accumulation over time. Right: Gamma-ray phase light curve folded with ephemeris (T_0 = 2450470.51140074 BJD, [2]) using photons from a 0.6° radius ROI.

5. Discussion and conclusion.

The initial observation of soft count spectra across the energy spectrum of 0.1-500 GeV hinted a potential emissions at lower energy levels, prompting a more focused analysis within the range of 50 MeV-20 GeV. This refined analysis uncovered several sources surpassing the Fermi detection threshold (TS>25), indicating the presence of significant gamma-ray emissions. Notably, our in-depth binned likelihood analysis, coupled with an exploration of pulsed emission modulated to the orbital period, revealed distinctive features in the gamma-ray light curves of polar systems. Through rigorous examination using Rayleigh tests, Tempo2, and H-test analyses, we identified potential periodicities in sources such as WW Hor , EF Eridani, EU UMa, AR UMa, and V834 Cen. The results contribute to an understanding of high-energy processes within these unique binaries. The observed gamma-ray emissions and identified periodicities offer valuable clues about the underlying astrophysical emission mechanisms governing polar systems.

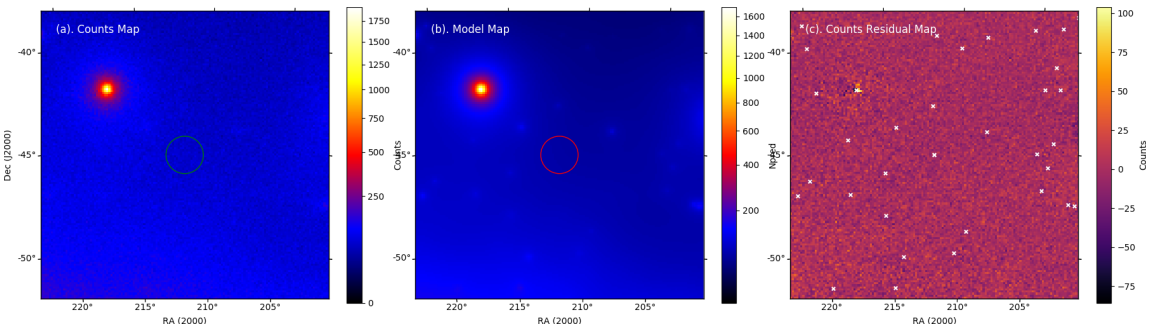

Figure 9: Displayed from the left is observed counts map of the source V834 Cen, the middle is the model counts map, and on the last panel is the residual map. All significant sources included in the model will show with their predicted counts in the model map. The residual map display the goodness of the fit. The difference between predicted and observed counts is reflected as either negative or positive counts at the locations where counts are underestimated or overestimated.

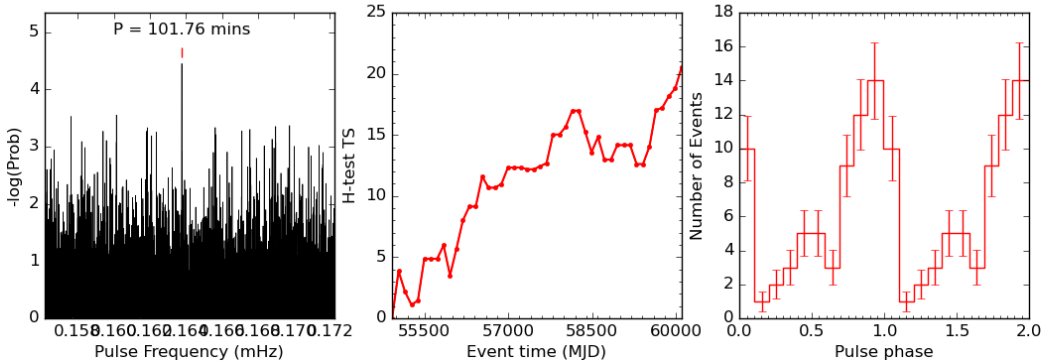

Figure 10: V834 Cen - Left: Rayleigh test power spectrum. Middle: H-test plot showing TS accumulation over time. Right: Gamma-ray phase light curve folded with ephemeris (T_0 = 2445048.07049723 BJD, [27]) using photons from a 0.6° radius ROI.

References

[1] G. Chanmugam and G. Dulk, *Am herculis binaries: Particle acceleration, radio emission and synchronization*, in *International Astronomical Union Colloquium*, vol. 72, pp. 223–227, Cambridge University Press, 1983.

[2] G. D. Schmidt, *Accretion in high magnetic fields: The stellar interaction*, in *Annapolis Workshop on Magnetic Cataclysmic Variables*, vol. 157, p. 207, 1999.

[3] M. Cropper, *The polars*, *Space Science Reviews* **54** (1990) 195.

[4] B. Warner, *Cataclysmic Variable Stars, Cambridge University Press, Cambridge*. 1995.

[5] G. Chanmugam and A. Ray, *The rotational and orbital evolution of cataclysmic binaries containing magnetic white dwarfs*, *The Astrophysical Journal* **285** (1984) 252.

[6] J. Kuijpers and J. Pringle, *Comments on radial white dwarf accretion*, *A&A* **114** (1982) L4.

[7] L. Chiappetti, E. G. Tanzi and A. Treves, *The system am her= 4u 1814+ 50*, *Space Science Reviews* **27** (1980) 3.

[8] S. T. Madzime, P. Meintjes, K. K. Singh and H. van Heerden, *Search for gamma-ray emission from the nova-like variable AE Aquarii using the Fermi-LAT Pass 8 data Archive*, in *Proceedings of 7th Annual Conference on High Energy Astrophysics in Southern Africa — PoS(HEASA2019)*, vol. 371, p. 051, 2020.

[9] S. Madzime, P. Meintjes, H. van Heerden, K. Singh, D. Buckley, P. Woudt et al., *The detection of pulsed emission at the spin-period of the white dwarf in ae aquarii in meerkat and fermi-lat data*, in *Proceedings of the 8th High Energy Astrophysics in Southern Africa (HEASA2021) Conference, Online*, pp. 13–17, 2021.

[10] S. T. Madzime, *The search for pulsed radio and gamma-ray emission from the cataclysmic variable system ae aquarii using meerkat and fermi-lat data*, Master's thesis, University of the Free State, 2021.

[11] Q. Kaplan, P. Meintjes and H. van Heerden, *Low-power pulsed emission at the spin period of the white dwarf in ar scorpii*, in *Proceedings of the 8th High Energy Astrophysics in Southern Africa (HEASA2021) Conference, Online*, pp. 13–17, 2021.

[12] Z. Arzoumanian, K. Gendreau, C. Baker, T. Cazeau, P. Hestnes, J. Kellogg et al., *The neutron star interior composition explorer (nicer): mission definition*, in *Space Telescopes and Instrumentation 2014: Ultraviolet to Gamma Ray*, vol. 9144, pp. 579–587, SPIE, 2014.

[13] P. Goldreich and D. Lynden-Bell, *Io, a jovian unipolar inductor*, *The Astrophysical Journal* **156** (1969) 59.

[14] W. Atwood, A. A. Abdo, M. Ackermann, W. Althouse, B. Anderson, M. Axelsson et al., *The large area telescope on the fermi gamma-ray space telescope mission*, *The Astrophysical Journal* **697** (2009) 1071.

[15] W. Atwood, A. Albert, L. Baldini, M. Tinivella, J. Bregeon, M. Pesce-Rollins et al., *Pass 8: toward the full realization of the fermi-lat scientific potential*, *arXiv preprint arXiv:1303.3514* (2013) .

[16] S. Abdollahi, F. Acero, L. Baldini, J. Ballet, D. Bastieri, R. Bellazzini et al., *Incremental fermi large area telescope fourth source catalog*, *The Astrophysical Journal Supplement Series* **260** (2022) 53.

[17] J. R. Mattox, D. Bertsch, J. Chiang, B. Dingus, S. Digel, J. Esposito et al., *The likelihood analysis of egret data*, *The Astrophysical Journal* **461** (1996) 396.

[18] P. S. Ray, M. Kerr, D. Parent, A. Abdo, L. Guillemot, S. Ransom et al., *Precise γ-ray timing and radio observations of 17 fermi γ-ray pulsars*, *The Astrophysical Journal Supplement Series* **194** (2011) 17.

[19] G. Hobbs, R. Edwards and R. Manchester, *Tempo2, a new pulsar-timing package–i. an overview*, *Monthly Notices of the Royal Astronomical Society* **369** (2006) 655.

[20] K. Beuermann, H. Thomas, P. Giommi and G. Tagliaferri, *Letter to the editor exo 023432-52323*, *Astron. Astrophys* **175** (1987) L9.

[21] J. Bailey, D. Wickramasinghe, J. Hough and M. Cropper, *Exo 023432–5232.3–an eclipsing am herculis binary*, *Monthly Notices of the Royal Astronomical Society* **234** (1988) 19P.

[22] K. Beuermann, P. Wheatley, G. Ramsay, F. Euchner and B. Gänsicke, *Evidence for a substellar secondary in the magnetic cataclysmic binary ef eridani*, *arXiv preprint astro-ph/0001183* (2000) .

[23] M. Cropper, *Simultaneous linear and circular polarimetry of ef eri*, *Monthly Notices of the Royal Astronomical Society* **212** (1985) 709.

[24] K. Beuermann, F. Euchner, K. Reinsch, S. Jordan and B. Gänsicke, *Zeeman tomography of magnetic white dwarfs-iv. the complex field structure of the polars ef eridani, bl hydri and cp tucanae*, *Astronomy & Astrophysics* **463** (2007) 647.

[25] T. Somova, N. Somov, J. Bonnet-Bidaud and M. Mouchet, *Spectroscopic and photometric studies of the magnetic cataclysmic variable eu uma (= re1149+ 28)*, *Astronomy Letters* **29** (2003) 31.

[26] S. B. Howell, M. M. Sirk, R. F. Malina, J. Mittaz and K. Mason, *Asymmetric mass accretion in the magnetic cataclysmic variable re 1149+ 28*, *The Astrophysical Journal* **439** (1995) 991.

[27] M. Cropper, J. Menzies and S. Tapia, *E1405–451: three seasons of polarimetry and photometry*, *Monthly Notices of the Royal Astronomical Society* **218** (1986) 201.